Assembly of the Major Light-Harvesting Complex II in Lipid Nanodiscs

Anjali Pandit,[†*] Nazhat Shirzad-Wasei,[‡] Lucyna M. Wlodarczyk,[†] Henny van Roon,[†] Egbert J. Boekema,[§] Jan P. Dekker,[†] and Willem J. de Grip[‡¶]

[†]Section of Biophysics, Faculty of Sciences, VU University Amsterdam, Amsterdam, The Netherlands; [‡]Department of Biochemistry, Nijmegen Centre for Molecular Life Sciences, Radboud University Nijmegen Medical Centre, Nijmegen, The Netherlands; [§]Department of Biophysical Chemistry, Groningen Biomolecular Sciences and Biotechnology Institute, Faculty of Mathematics and Natural Sciences, University of Groningen, Groningen, The Netherlands; and [¶]Department of BioOrganic Physical Chemistry, Leiden Institute of Chemistry, Leiden University, Leiden, The Netherlands

ABSTRACT Self-aggregation of isolated plant light-harvesting complexes (LHCs) upon detergent extraction is associated with fluorescence quenching and is used as an in vitro model to study the photophysical processes of nonphotochemical quenching (NPQ). In the NPQ state, in vivo induced under excess solar light conditions, harmful excitation energy is safely dissipated as heat. To prevent self-aggregation and probe the conformations of LHCs in a lipid environment devoid from detergent interactions, we assembled LHCII trimer complexes into lipid nanodiscs consisting of a bilayer lipid matrix surrounded by a membrane scaffold protein (MSP). The LHCII nanodiscs were characterized by fluorescence spectroscopy and found to be in an unquenched, fluorescent state. Remarkably, the absorbance spectra of LHCII in lipid nanodiscs show fine structure in the carotenoid and Q_y region that is different from unquenched, detergent-solubilized LHCII but similar to that of self-aggregated, quenched LHCII in low-detergent buffer without magnesium ions. The nanodisc data presented here suggest that 1), LHCII pigment-protein complexes undergo conformational changes upon assembly in nanodiscs that are not correlated with downregulation of its light-harvesting function; and 2), these effects can be separated from quenching and aggregation-related phenomena. This will expand our present view of the conformational flexibility of LHCII in different microenvironments.

INTRODUCTION

The photosystem II (PSII) antenna can switch from a fluorescent to a fluorescence-quenched state under intense illumination in a process called nonphotochemical quenching (NPQ). In this photoprotective mode, the light-harvesting antennae are involved in downregulation of photosynthesis and harmful light energy is rapidly dissipated as heat (1). The fluorescence-quenched state can be induced in vitro in aggregated major or minor antenna complexes, and a comparison of the pigment's spectroscopic properties strongly suggests that the in vitro and in vivo photophysical mechanisms are similar (2,3). However, the origin of the photophysical processes that lead to the NPQ state is the subject of much debate, and several mechanisms have been proposed for the associated reversible switch in pigment configuration. It has been suggested that a carotenoid radical cation acts as a quencher of the chlorophyll excited states (4), and that conformational changes in the minor antennae can modulate the chlorophyll-zeaxanthin (Chl-Zea) charge-transfer quenching (5). Alternatively, Chl-Chl charge transfer states in LHCII oligomers were proposed to be an intermediate for the fluorescence quenching process (6), characterized by a far-red emitting state (7). Several studies suggested that fluorescence quenching is induced by conformational changes in the major LHCII antenna. The occurrence of a conformational change in this protein was demonstrated by resonance Raman, which showed a twist in the neoxanthin (Neo) carotenoid when the antenna system switched from a light-harvesting to an energy-dissipating state in vivo (3). Similar Raman features are observed upon self-aggregation of LHCII, which induces fluorescence quenching in vitro. It was proposed that the protein conformational change alters the interaction between a lutein (Lut) and Chl, transferring the light energy from Chl to a low-lying carotenoid excited state in the energy-dissipating mode (3). Another model, also based on Car S1-Chl interactions, suggests a photophysical mechanism in which short-living, low excitonic carotenoid chlorophyll states serve as traps and dissipation valves for excess excitation energy (8,9).

In the work of Ilioaia et al. (10), LHCII fluorescence quenching was induced by extraction of detergent from isolated LHCII proteins entrapped in gels, which precludes protein aggregation. The results strongly support the concept that the process of fluorescence quenching is caused by intramolecular conformational changes rather than protein aggregation per se (10). In a recent study involving single-molecule fluorescence experiments on isolated LHCII trimers, spectral fluctuations were attributed to small conformational changes in the pigment-protein scaffold (11). The conformational diffusion of single LHCII trimers is controlled by the local environment, which can shift the dynamic equilibrium between strongly and weakly fluorescing states (12). The level of fluorescence quenching in in vitro aggregates is modulated by a variety of factors, including the detergent concentration, pH, ionic strength, and Mg concentration (13–15). In addition, it was recently shown that the quenching behavior and aggregate size of

Submitted June 10, 2011, and accepted for publication September 27, 2011.

*Correspondence: a.pandit@vu.nl

Editor: Leonid S. Brown.

© 2011 by the Biophysical Society

0006-3495/11/11/2507/9 $2.00

doi: 10.1016/j.bpj.2011.09.055

LHCII complexes depend on the presence of different thylakoid membrane lipids (16).

Few studies have concentrated on the mechanism of NPQ in liposome-reconstituted photosystem II (PSII) antenna complexes that mimic protein-lipid interactions (17,18). In such systems, protein aggregation and the degree of fluorescence quenching are not easily controlled. Thus, the effects of self-aggregation, conformational switching, and protein-lipid interactions, all of which have been suggested to play a role in the mechanism of NPQ, are not easily measured independently.

Here, we introduce what to our knowledge is a new platform to study the behavior of single light-harvesting complexes (LHCs) in a lipid environment. We assembled LHCII trimer complexes into lipid nanodiscs (nanometer-sized lipid bilayer discs surrounded by a membrane scaffold protein (MSP)) (19). We used two types of MSPs (MSP-E3D1 (20) and ZAP1 (21)) that, according to their lengths, can form nanodiscs with ~12 nm and ~10 nm diameters. A schematic picture of a lipid nanodisc and the size of the LHCII trimer complex inside a 12 nm nanodisc is shown in Fig. 1. Under optimized conditions, assembly of LHCII trimers into E3D1 and ZAP1 membrane discs formed nanodiscs with 12–14 nm and 10–15 nm diameters, respectively. The fluorescence yields of the LHCII-E3D1 nanodiscs were found to be comparable to those of LHCII trimer complexes solubilized in buffered detergent solution. Interestingly, the absorbance and fluorescence excitation spectra were not identical to detergent-solubilized LHCII with respect to fine structure in the Soret and Q_y regions. We hypothesize that substituting detergent for lipid interactions induces conformational changes that are unrelated to quenching or aggregation phenomena, illustrating the conformational flexibility of LHCII pigment-protein complexes in different microenvironments.

MATERIALS AND METHODS

Overexpression and purification of the MSPs E3D1 and ZAP1

The plasmid for ZAP1 (21) was a kind gift from Drs. S. Banerjee and T.P. Sakmar (Rockefeller University, New York), and the plasmid MSP1E3D1 (22,23) was obtained from Addgene (Cambridge, MA). Both cDNA constructs were N-terminally extended with a His-tag and cloned into a pET28a plasmid with a kanamycin-resistant backbone. The purified plasmids were transformed into competent BL21 (DE3) *Escherichia coli, Rosetta*2 strain (EMD Biosciences, Darmstadt, Germany), and plated on LB-agar containing appropriate antibiotics. A single colony was grown overnight at 37°C in 30 ml LB medium containing 30 μg/ml kanamycin with shaking at 180 rpm to generate a starter culture. The starter culture was added to 0.5–1 liter of Terrific Broth (TB) medium (Sigma-Aldrich, St. Louis, MO) and incubated at 37°C with shaking at 180 rpm until an OD_{585} of 0.6–0.7 was reached. MSP production was induced by adding isopropyl β-D-1-thiogalactopyranoside (IPTG) to a final concentration of 1 mM. The cells were harvested 3–4 h after induction by centrifugation (3000 $\times$ g, 30 min). The cell pellet was resuspended in storage buffer (40 mM Tris, 0.3 M NaCl, 2 mM phenylmethanesulfonylfluoride, 5 mM 2-mercaptoethanol, and one tablet per 50 ml complete EDTA-free protease inhibitor (Hoffman-La Roche AG, Basel, Switzerland) in MilliQ, pH 8.0) and stored at −80°C.

The stored cell pellet was thawed on ice, and lysozyme (12.5 mg/500 ml culture; NBC Cleveland, OH) and Benzonase Nuclease (3 μl/500 ml culture, purity > 99%; EMD Biosciences) were added. After 30 min of incubation on ice, Tergitol-type NP-40 (10%; Sigma-Aldrich) was added at 125 μl/500 ml culture. The suspension was sonicated five times for 45 s under ice-cooling to disrupt the cells, followed by centrifugation (3000 $\times$ g, 30 min, 4°C). We purified the MSP from the supernatant using immobilized metal affinity chromatography exploiting the His-tag, in a batchwise procedure modified from (23,24). The supernatant was incubated overnight under rotation at 4°C with Ni-NTA Superflow beads (Qiagen, Qiagen Benelux B.V., Venlo, The Netherlands; 6 ml beads per liter of culture) that were preequilibrated with buffer A (40 mM Tris, 0.3 M NaCl, 1 mM NaN_3, pH 8.0). The loaded beads were then washed sequentially with the following volumes and buffers: 3 bead volumes (BV) of buffer B (40 mM Tris, 0.3 M NaCl, 1% NP-40, pH 8.0), 3 BV of buffer C (40 mM Tris, 0.3 M NaCl, pH 8.0), 3 BV of buffer D (40 mM Tris, 0.3 M NaCl, 20 mM imidazole, pH 8.0), and 0.5 BV of buffer A with 50 mM imidazole. The MSP was then eluted several times with 0.5 BV of buffer A with 200 mM imidazole until the A280 was reduced substantially, and finally two or three times with 0.5 BV of buffer A with 400 mM imidazole to complete the elution. The purified protein was assayed for purity via SDS-PAGE and silver staining, and the fractions were stored at −20°C.

This procedure produced two bands for ZAP1 at ~30 and 26 kDa, both of which are competent in nanodisc formation, and one band for E3D1 at 32 kDa. We determined the MSP concentration from the A280 using a molar absorbance of 23,000 $Mol^{-1}.cm^{-1}$ for ZAP1 (21) and 29,900 $Mol^{-1}.cm^{-1}$ for E3D1 (23). The yield of purified MSP varied between 100 and 200 mg/liter of culture.

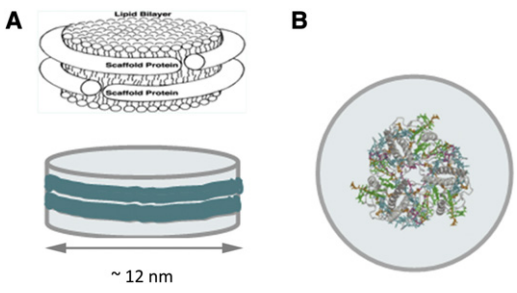

FIGURE 1 Schematic picture (*A*) of a lipid nanodisc formed by a dimer of two membrane scaffold proteins and (*B*) top view of the LHCII trimer complex scaled inside a 12-nm nanodisc.

LHCII isolation

We isolated trimeric LHCII complexes from spinach as previously described (25) using anion-exchange chromatography and the detergent *n*-dodecyl β-D-maltoside (β-DM) for solubilization of the complexes.

Preparation of LHCII-lipid nanodiscs

For incorporation of the LHCII in lipid nanodiscs, the LHCII complexes solubilized in DM were first mixed with soy asolectin lipids (Sigma) solubilized in β-nonylglucoside (NG) to a final molar ratio of LHCII/lipid/detergent of 1:60:420, taken the NG and β-DM together. The mixture was incubated for 15 min. Subsequently, the MSP E3D1 or ZAP1 was added to a final LHCII/MSP ratio of 1:2, 1:3, or 1:6, and the mixture was again incubated for 15 min. As a control, we prepared a sample in which no scaffold proteins were added in this step. Detergent extraction, leading

to the assembly of LHCII-MSP lipid nanodiscs or proteoliposomes in the control sample, was accomplished by complex formation with heptakis (2,6-di-O-methyl)-β-cyclodextrin (Sigma-Aldrich), added as a solid in one step or in three steps to a final molar ratio of 1:1 cyclodextrin/detergent (26). The samples were incubated for 45 min in total and finally subjected to centrifugation (80,000 $\times$ g, 30 min, 4°C) to separate the nanodiscs from any large aggregates and liposomal material. The collected supernatant was dialyzed against detergent-free buffer (20 mM Hepes/KOH, pH 7.8, 10 mM NaCl, and 3 mM EDTA) for removal of the cyclodextrin-detergent complexes and stored at −80°C until further use. The control sample without MSP proteins would form LHCII-containing proteoliposomes that were collected from the pellet. The absorbance spectra of the control before and after centrifugation show that no free LHCII is present in the supernatant (see Fig. S1 in the Supporting Material), confirming that the LHCII complexes were taken up by the lipid membranes or sedimented as LHCII aggregates. All steps were performed at 4°C.

Steady-state absorbance and fluorescence spectroscopy

We measured fluorescence excitation and emission spectra using a commercial spectrophotometer (Jobin Yvon, Fluorolog) with excitation and emission bandwidths of 2 nm. The LHCII nanodiscs were diluted in buffer containing 20 mM Hepes/KOH, pH 7.8, 10 mM NaCl, and 3 mM EDTA, and measured in 1$\times$1 cm cuvettes. To prevent potential aggregation of the LHCII nanodiscs through stacking interactions, we added no $MgCl_2$. For 77K measurements, the LHCII nanodiscs were diluted in 40% Hepes buffer and 60% glycerol (v/v) and cooled in a nitrogen-bath cryostat to 77K. We measured absorbance spectra on a Cary 50 spectrophotometer, using a 1 nm slit width for the absorbance wavelength and a path length of 1 cm. We determined the room-temperature fluorescence quantum yields (QY) of the samples relative to LHCII in buffered 0.03% β-DM solution by comparing the room-temperature transmission (1-T) and steady-state fluorescence spectra of the respective samples.

Time-resolved fluorescence spectroscopy

Time-resolved emission measurements were performed at room temperature with a Streak camera setup. The samples were placed into a 1$\times$1 cm quartz cuvette and stirred continuously while excitation was performed at the very edge of the cuvette. The absorbance of the sample was 0.1–0.15 at 400 nm. We generated excitation pulses of 400 nm (~100 fs) with vertical polarization using a titanium:sapphire laser (Coherent, Santa Clara, CA) with a regenerative amplifier (Coherent, MIRA seed and RegA) that was used to pump an optical parametric amplifier (Coherent, OPA). The repetition rate was 50 kHz with pulse energy of 0.2 nJ in the sample, which resulted in $<$0.05% excited Chls per pulse. The data were analyzed with the use of global analysis techniques (27).

Electron microscopy

LHCII nanodiscs were prepared by the negative staining method with 2% uranyl acetate (28). Electron microscopy was performed on a Philips CM120 transmission electron microscope (FEI, Eindhoven, The Netherlands) operated at 120 kV.

RESULTS

Morphological characterization of the LHCII nanodisc preparations

The electron micrograph pictures of the different preparations show that at the highest molar ratio of E3D1/LHCII (6:1), homogeneous discs of 12–14 nm diameter are formed (Fig. 2 *A*), matching the length of the E3D1 scaffold protein (23). Under the same conditions, the ZAP1/LHCII disc preparation showed a more variable size distribution, ranging from 10 to 20 nm, with an average diameter of 15 nm (Fig. 2 *B*). We could not distinguish the LHCII trimers inside the discs by negative-staining electron microscopy (EM), probably because the major part of the LHCII protein is embedded inside the membrane matrix in the discs. Atomic force microscopy studies on bacteriorhodopsin (Br) nanodiscs have shown that incorporating membrane proteins can increase the disc sizes compared with empty discs (29). We presume, therefore, that the ZAP1 nanodiscs of ~10 nm diameter represent empty discs enclosed by a single dimer of ZAP1 proteins (21), and the larger discs contain LHCII. The control experiment performed without addition of MSP resulted in larger proteoliposomes with a strong tendency to stack together (Fig. 3).

Reducing the MSP/LHCII ratio resulted in inhomogeneous mixtures of small discs (10–15 nm), larger discs (20–40 nm), and disc-shaped particles (~100 nm; not shown). The diameters of the intermediate-sized discs are a multiple of 10 and 12 nm, which suggests that these discs are formed by a multiple of MSP dimers. During the detergent removal step in the LHCII-nanodisc sample, two processes compete with each other: the LHCII complexes have a high tendency to self-aggregate, whereas the MSPs associate with lipids or lipid-LHCII mixtures to form closed discs that prevent further self-aggregation. The outcome of these two processes will strongly depend on their kinetics, and hence on the MSP/LHCII ratio. In the case of LHCII, this ratio has to be raised to 6:1 to largely prevent LHCII self-aggregation. For proteins with a low tendency to aggregate, this ratio can be lowered (23). For instance, we found that using a 2:1 molar ratio of E3D1 to reaction center (RC) protein produced homogeneous 13-nm particles, as determined by dynamic light scattering (not shown).

Spectral properties of the LHCII nanodisc preparations

Room-temperature absorbance and fluorescence spectra of the LHCII-nanodisc preparations confirmed that the LHCII complexes were in a well-folded, functional state inside the nanodisc membrane matrix, exhibiting fluorescence energy transfer among the LHCII pigments. The inhomogeneous preparations had a decreased fluorescence QY, consistent with the idea that they consist of a mixture of small discs with unquenched single LHCII trimers together with larger discs and sheets with fluorescence-quenched LHCII aggregates. Fig. 4 shows the 77K fluorescence emission spectra of the different preparations. The fluorescence intensity was scaled to the fluorescence maxima around 678 nm. The inset shows the fluorescence peak that is ~0.5 nm red-shifted for the homogeneous LHCII-ZAP1 and LHCII-E3D1 1:6

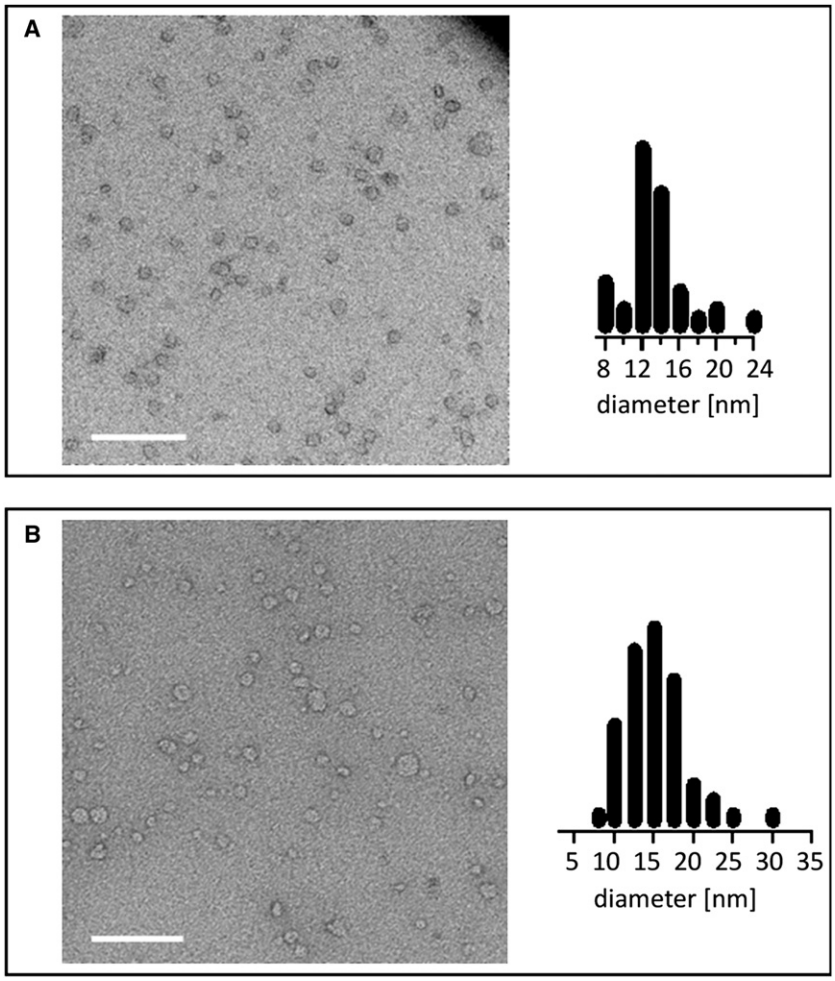

FIGURE 2 Electron micrographs of the (*A*) LHCII-E3D1 nanodiscs and (*B*) LHCII-ZAP1 nanodiscs prepared at an MSP/LHCII ratio of 1:6. The scale bar is 100 nm.

preparations, and further red-shifted for the inhomogeneous LHCII-nanodisc preparations and the LHCII proteoliposomes. The room-temperature fluorescence QYs relative to LHCII in buffered 0.03% β-DM solution are indicated in the figure. The spectra of the inhomogeneous preparations contained a distinct shoulder at 700 nm. The ratio between the 680 and 700 nm band is commonly used as a measure for aggregate formation (30). Interestingly, the F700/F680 peak ratio of the LHCII-ZAP1 1:2 was substantially lower than in the control sample with LHCII proteoliposomes (0.22 vs. 0.38), although the fluorescence yields relative to unquenched LHCII were similar (0.40 vs. 0.37). This suggests that the fluorescence 700 nm emission band at 77K and the fluorescence quenching at room temperature are not strictly correlated.

Fig. 5 shows the room-temperature absorbance spectra of the homogeneous LHCII-ZAP1 and LHCII-E3D1 nanodiscs, and LHCII trimers solubilized in 0.03% β-DM. The spectra were normalized at 405 nm because there are no apparent changes in this region, and the spectra are less affected by light scattering in this region than in the region below 400 nm. This normalization procedure is somewhat arbitrary, but it allows a good comparison of the subtle changes in the spectral properties of the various preparations. Significant spectral differences between LHCII in β-DM and the nanodiscs are observed in the Soret, carotenoid, and Q_y regions. Fig. 6 shows the absorbance difference spectra obtained by subtracting the normalized absorbance spectra of LHCII solubilized in 0.03% β-DM from those of the LHCII nanodiscs. In the Soret region, most prominent in all spectra are negative bands around 416 and 444 nm, and in the range of 472–486 nm. The spectra in the Q_y region show a positive band at 661 and a negative band at 676 nm. The spectra are remarkably similar to the spectra of aggregated LHCII in low-detergent buffer without magnesium ions (Mg, shown in trace 5 in the same figure) except for the lack of an additional positive band at 683 nm in the Q_y region. The bottom trace (trace 6) in Fig. 6 presents the difference spectrum of aggregated LHCII in highly diluted detergent solution in the presence of 5 mM $MgCl_2$. This trace clearly shows that upon Mg addition, a broad band at 500 nm appears and the positive band at 683 nm is much more pronounced. The difference spectrum in trace 6 resembles the absorbance difference

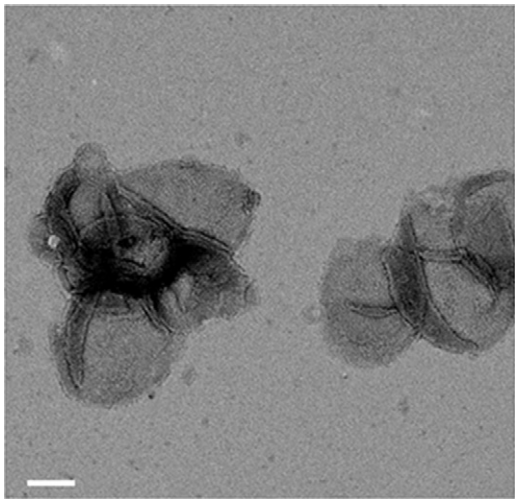

FIGURE 3 Electron micrograph of the control sample prepared without MSP. The scale bar is 100 nm.

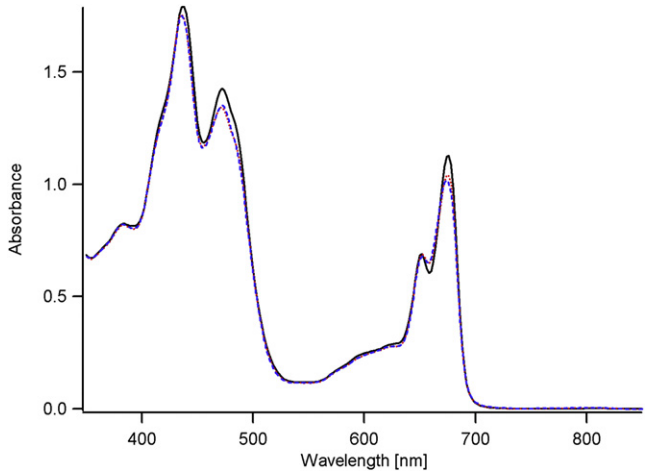

FIGURE 5 Room-temperature absorbance spectra of the LHCII-E3D1 (*red*, *dotted*) and LHCII-ZAP1 (*blue*, *dashed*) nanodiscs prepared with an LHCII/MSP ratio of 1:6, and unquenched LHCII trimers solubilized in 0.03% β-DM (*black solid line*). The spectra are normalized at 405 nm.

spectra of aggregated LHCII reported by Ruban et al. (31). In addition, the fluorescence is further quenched with the QY relative to unquenched LHCII trimers, decreasing from 0.28 to 0.13. In contrast, addition of $MgCl_2$ over a range of 1–40 mM to a solution with LHCII in nanodiscs did not significantly affect the absorbance spectra or the fluorescence QY (not shown), and no changes were observed in the LHCII nanodisc particle size distribution in EM micrographs.

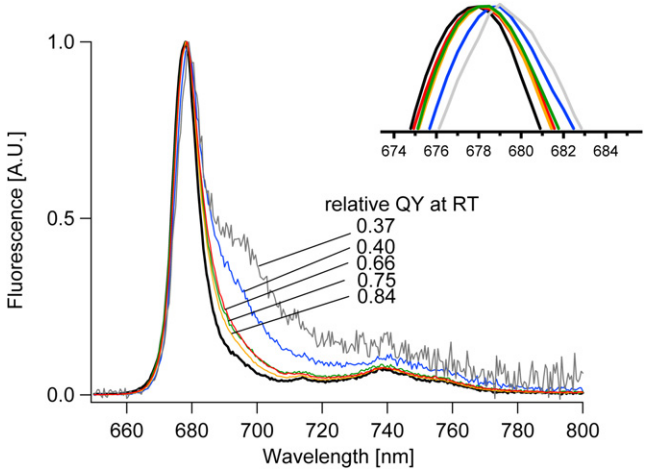

FIGURE 4 77K fluorescence emission spectra of LHCII-ZAP1 1:2 (LHCII/MSP) (*blue*, RT QY = 0.40), LHCII-E3D1 1:2 (*red*, RT QY = 0.66), LHCII-ZAP1 1:6 (*green*, RT QY = 0.75), and LHCII-E3D1 1:6 (*orange*, RT QY = 0.84), and the control sample containing LHCII proteoliposomes (*gray*, RT QY = 0.37). The thick-lined black spectrum is of LHCII trimers solubilized in 0.03% β-DM buffer. RT QY is the room-temperature fluorescence QY relative to LHCII trimers in 0.03% β-DM. The inset shows the emission peaks around 680 nm, with (from left to right) LHCII trimers in 0.03% β-DM, LHCII-E3D1 1:6, LHCII-E3D1 1:2, LHCII-ZAP1 1:6, LHCII-ZAP1 1:2, and LHCII proteoliposomes.

Similar features were detected in the 77K fluorescence excitation spectra (Fig. 7). The fluorescence excitation spectra, which are less affected by light scattering than the absorbance spectra, were normalized at 380 nm. Fig. 8 shows the 77K fluorescence excitation difference spectra, based on the normalized fluorescence spectra of LHCII in Fig. 7 and obtained by subtracting LHCII solubilized in 0.03% β-DM from those of the LHCII nanodiscs or from the control LHCII proteoliposomes. Both the ZAP1 and E3D1 nanodiscs in the homogeneous and inhomogeneous preparations, as well as the control sample containing LHCII in proteoliposomes, again show fine structure in the

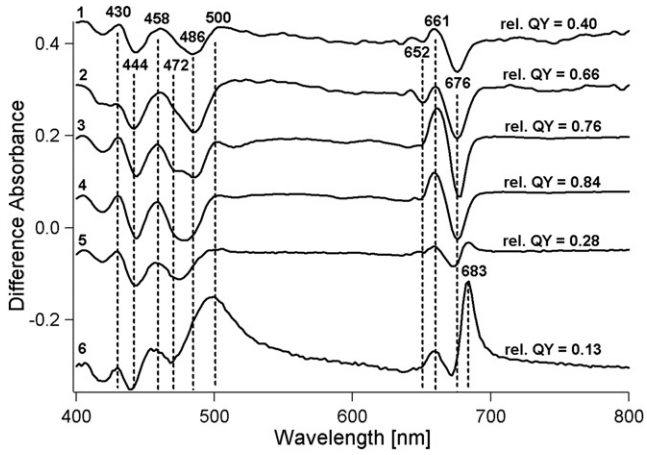

FIGURE 6 Room-temperature absorbance difference spectra of (trace 1) LHCII-ZAP1 1:2, (trace 2) LHCII-E3D1 1:2, (trace 3) LHCII-ZAP1 1:6, and (trace 4) LHCII-E3D1 1:6 nanodiscs, and LHCII aggregates in 0.0003% β-DM buffer prepared (trace 5) without Mg and (trace 6) with 5 mM $MgCl_2$, obtained by subtracting the absorbance of unquenched LHCII in 0.03% β-DM. QY values are relative to the QY of LHCII trimers in 0.03% β-DM. The original absorbance spectra were normalized at 405 nm.

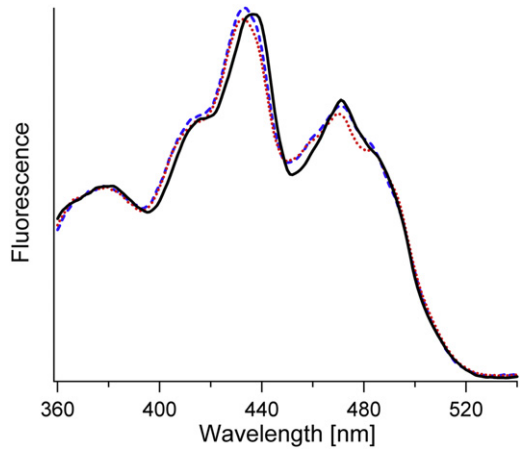

FIGURE 7 77K fluorescence excitation spectra of the LHCII-E3D1 (*red*, *dotted*) and LHCII-ZAP1 (*blue*, *dashed*) nanodiscs prepared with an LHCII/MSP ratio of 1:6, and unquenched LHCII trimers solubilized in 0.03% β-DM (*black solid line*). The emission wavelength was 680 nm. The spectra are normalized at 380 nm.

difference spectra with negative bands at 416, 441, 470–472, and 488 nm. For completeness, we note that normalizing the fluorescence spectra at 405 nm (as was done for the absorbance spectra) did not change these wavelengths, and only shifted the baseline of the difference spectra. Because the control sample (proteoliposomes) had a low signal/noise ratio, its spectrum was smoothed with a binomial fit, and both the original spectrum (*dotted line*) and the smoothed spectrum (*solid line*) are presented.

For the 1:6 LHCII/MSP disc preparations of the E3D1 and ZAP1 nanodiscs, the fluorescence lifetimes were probed

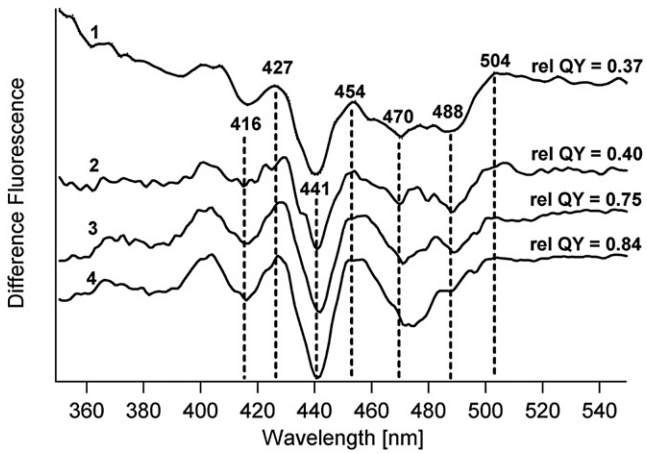

FIGURE 8 77K fluorescence excitation difference spectra of (trace 1) the control sample containing LHCII proteoliposomes, (trace 2) LHCII-ZAP1 1:2 (LHCII/MSP), (trace 3) LHCII-ZAP1 1:6, and (trace 4) LHCII-E3D1 1:6 nanodiscs, obtained by subtracting the 77K excitation spectrum of unquenched LHCII in 0.03% β-DM. The emission wavelength was 680 nm. QY is the room-temperature fluorescence QY relative to LHCII trimers in 0.03% β-DM. The original fluorescence excitation spectra were normalized at 380 nm.

with a Streak camera system and compared with those of detergent-solubilized LHCII. The LHCII E3D1 and ZAP1 nanodiscs had a major component lifetime of 3.3–3.5 ns and a smaller 340–390 ps component, whereas the detergent-solubilized LHCII had a dominant lifetime component of 3.5 ns with a very small contribution of a 1.3 ns component (Fig. 9 and Table 1).

DISCUSSION

A comparison of the two types of MSP shows that only the larger E3D1 protein yielded very homogeneous LHCII-nanodisc preparations with a size distribution that can be expected from the length of this MSP (23). We presume that a minimal disc size of ~12 nm diameter is necessary for proper incorporation of LHCII trimers into the discs, and that the use of a smaller MSP, such as ZAP1, leads to discs that cannot be smoothly fit with a single MSP dimer, allowing less control over the final LHCII-nanodisc structure. In addition, because of the tendency of LHCII to self-aggregate, one must ensure high MSP/LHCII ratios to obtain homogeneous LHCII nanodiscs. It is interesting to also note the formation of discs whose diameter sizes are a multiple of the MSP lengths. This suggests that by optimizing the LHCII nanodisc preparation protocol and adding subsequent purification steps, one might also obtain a set of small LHCII aggregates of discrete sizes.

From the fluorescence data we obtained for the homogeneous LHCII-E3D1 nanodisc samples, we can conclude that the LHCII trimers incorporated inside the nanodiscs are not subject to quenching of their fluorescence. The small (~340 ps) lifetime component in the fluorescence decay could reflect small impurities with small (i.e., $<$100 nm) LHCII aggregates. No large particles were observed in this sample in the electron micrographs, which suggests that substantial quenching can be induced in small aggregates. Global analyses of the streak image spectra of LHCII solubilized in 0.03% β-DM reveals a dominant 3.5 ns

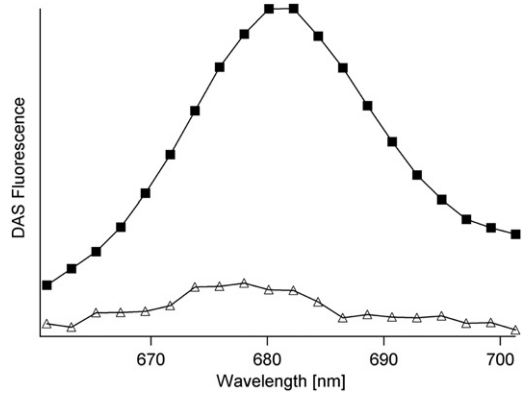

FIGURE 9 Decay-associated spectra of the 3.5 ns fluorescence lifetime component (*solid squares*) and 0.34 ns component (*open triangles*) of LHCII-E3D1 nanodiscs prepared with a LHCII/MSP ratio of 1:6.

TABLE 1 The fluorescence lifetimes and corresponding decay-associated spectra amplitudes of LHCII trimers in detergent and of LHCII trimers in the lipid nanodiscs, prepared with an LHCII/MSP ratio of 1:6

Sample	τ_{fluor} (ns)	Amplitude
LHCII in 0.03% β-DM	3.4	0.99
	1.3	0.01
LHCII-E3D1	3.5	0.89
	0.3	0.11
LHCII-ZAP1	3.3	0.80
	0.4	0.20

component, whereas two long lifetime components of ~2 and 3.8 ns were measured for unquenched LHCII trimers via photon counting techniques (32). This could reflect the fact that Streak images only directly probe the first 1.5 ns after the excitation pulse, and longer lifetimes are estimated with the use of the back sweep (27). For Chl in natural membranes in unquenched states, shorter lifetimes (~2 ns) have been reported (33,34), and similar lifetimes were reported for the longest lifetime component of LHCII reconstituted in proteoliposomes (17). In the study by Moya et al. (17), the fluorescence quenching was shown to depend on the lipid/protein ratio, and the average lifetime decreased from ~2 ns to ~1 ns when the lipid/protein ratio was decreased from 6.6 to 2.2 (mole/moles). This was ascribed to protein-protein interactions at low lipid/protein ratios, which lead to a strong increase in the amplitude of a ~0.3 ns lifetime component. The fact that the fluorescence of single LHCII trimers embedded in lipid nanodiscs has a dominant lifetime component of 3.5 ns suggests that the shorter ~2 ns Chl lifetime observed in vivo or for LHCII reconstituted in proteoliposomes results from protein-protein contacts between trimers, crowding, and/or induced lateral pressure in natural membranes. We did not attempt here to mimic photosynthetic membranes by using natural lipid compositions, and we also presume that lipid packing is less rigid in small nanodiscs than in crowded photosynthetic membranes that are densely packed with proteins.

Considering that the homogeneous preparations of LHCII in 12–14 nm lipid nanodiscs are unquenched and in a nonaggregated state, it is remarkable that the difference in electronic absorbance compared with detergent-solubilized LHCII shows fine structure that in the Soret, carotenoid, and Q_y regions is similar to aggregated LHCII diluted in low-detergent buffers without Mg^{2+} ions. In addition, no clear correlation is observed between the amplitude of the peaks and the decrease in the fluorescence QY. This strongly suggests that the observed absorbance spectral changes in our samples are not caused by aggregation or quenching. Because the nanodisc diameter is only about twice that of a LHCII trimer, we cannot exclude the possibility that the LHCII protein interacts with the MSP scaffold protein, resulting in the observed spectral changes. A comparison of the behavior of LHCII inside lipid nanodiscs with studies of LHCII in liposomes prepared at very high lipid/protein ratios, and under conditions that stringently avoid LHCII aggregation, could be useful for assessing the possibility of LHCII-MSP interactions. Recently, Grinkova et al. (35) successfully designed extended MSP constructs that form larger nanodiscs of ~17 nm diameter. The use of these extended MSPs, if they are carefully prepared to avoid incorporation of more than one trimer per nanodisc, could be an alternative way to reduce any LHCII-MSP interaction, because they are less likely to occur in nanodiscs of increased size.

However, the similarity of the LHCII-nanodisc absorbance difference spectra with the difference spectra of LHCII aggregates prepared in buffer without Mg suggests that the observed spectral changes reflect the effects of extracting detergent and substituting the detergent shell for LHCII-lipid or LHCII protein-protein contacts. The positive band at 683 nm in the Q_y region is absent for all LHCII nanodisc preparations. This 683 nm band and the 500 nm band are much more enhanced in difference spectra of aggregated LHCII upon addition of Mg. It is well known that Mg induces stacking of thylakoid membranes in vivo (36,37) and the addition of >100 μM $MgCl_2$ induces stacking and enhanced lateral aggregation of LHCII in vitro (15). The increased sizes of the LHCII aggregates in Mg buffer may very well lead to absorbance flattening, and the difference spectra may be subjected to absorbance artifacts in the form of flattening-related distortions (38,39).

The bottom spectrum in Fig. 6 of aggregated LHCII in the presence of 5 mM $MgCl_2$ resembles the difference in absorbance that has been reported for isolated LHCII in aggregated minus trimeric state in vitro, and for isolated thylakoids in the NPQ minus Fm state in vivo (30). The insensitivity of the electronic absorbance profile of LHCII trimers in nanodiscs to Mg suggests that the nanodisc compartmentalization prevents not only lateral self-association of LHCII but also Mg-mediated self-association into stacks. The resolution of the EM micrographs is not high enough to completely exclude stacking of nanodiscs into dimers in the presence of Mg, but it certainly can be concluded that no Mg-mediated large lateral or three-dimensional aggregates were formed in the nanodisc samples.

In contrast to the LHCII nanodiscs, the control sample contained fused LHCII proteoliposomes that might mediate stacking of LHCII. This could explain the difference in emission properties of the inhomogeneous nanodisc preparations and the proteoliposome control, with respect to the relation between the F700/F680 ratio in the 77K fluorescence spectrum and the room-temperature fluorescence QY.

The band at 500 nm that is strongly enhanced in aggregated LHCII in the presence of Mg corresponds to lutein 1 (Lut1) (1,40,41), The +/− bands at 676/661 nm in the Q_y region correspond to Chl *a*. These bands are more intense in the nanodisc spectra than in the spectra of aggregated LHCII, and correspond to a small blue shift in absorbance for LHCII in nanodiscs. This is in contrast to the red shift

that is observed both for aggregated LHCII and for chloroplasts in the NPQ state (42). The negative peak at 472 nm probably corresponds to Chl *b* and the band at 486 nm to neoxanthin (Neo) (1,41,43). The negative band at 444 nm could correspond to Chl *a* or to lutein 2 (Lut2). Conformational changes may occur near these pigment sites, inducing a change in the electronic states of Neo, Lut2 or Chl *a*, and Chl *b*.

The 77K fluorescence excitation difference spectra in Fig. 8 resemble the 77K fluorescence excitation difference spectra of chloroplasts in the NPQ minus Fm states (42) by having a negative band around 440 nm, which, however, is more pronounced for the LHCII nanodiscs, and a small negative shoulder at 488 nm, which is more pronounced for the chloroplasts in the NPQ state. The small shoulder at 488 nm could reflect small amounts of aggregated LHCII in the disc samples because its contribution is higher in preparations with a lower fluorescence yield. The 440 nm band, however, is more pronounced for the unquenched, homogeneous disc preparations. In that respect, it is noteworthy that a similar negative band observed in difference spectra of native membranes in NPQ minus Fm states is correlated with quenching-induced changes in the pigment or protein configuration. This suggests that the conformational space available to the LHCII trimer has specific substates that are shared by certain functional transitions.

More-extended experiments must be performed before we can characterize how LHCII protein conformational and pigment electronic states are modulated by the nanodisc assembly. Preliminary resonance Raman experiments suggest that conformational differences occur between LHCII in nanodiscs and detergent-solubilized or aggregated LHCII, demonstrating the conformational flexibility of the LHCII pigment-protein complex in adaptation to different microenvironments.

CONCLUSION

Lipid nanodiscs represent a new, to our knowledge, platform for studying isolated LHCs in a lipid environment that is devoid of detergent interactions while avoiding protein self-aggregation. Nanodisc samples are suitable for spectroscopic experiments in which light scattering should be diminished, and for single-molecule studies that require attachment to a substrate. In in vitro studies of the NPQ behavior of isolated light-harvesting proteins, one can induce fluorescence quenching by removing detergent from the buffer. To date, the effects of detergent removal and in vitro fluorescence quenching have not been characterized independently. Our first results from LHCII lipid nanodiscs show that LHCII trimer complexes embedded in the disc membranes are unquenched, but suggest that conformational changes occur when the LHCII proteins are transferred from a detergent to a lipid environment. Further experiments to spectroscopically characterize the protein and pigment conformations of LHCII in different microenvironments are currently in progress.

SUPPORTING MATERIAL

A figure is available at http://www.biophysj.org/biophysj/supplemental/S0006-3495(11)01189-1.

We thank Drs. S. Banerjee and T. P. Sakmar (Rockefeller University, New York) for the generous gift of the expression plasmid for ZAP1 and corresponding experimental advice, and Dr. M. C. A. Stuart (University of Groningen, Groningen, The Netherlands) for his technical assistance with the EM.

This work was supported by the HARVEST Marie Curie Research Training Network (PITN-GA-2009-238017) and the Council for Chemical Sciences of the Netherlands Foundation for Scientific Research (NWO-CW project 700.54.008).

REFERENCES

1. Palacios, M. A., R. N. Frese, …, H. van Amerongen. 2003. Stark spectroscopy of the light-harvesting complex II in different oligomerisation states. *Biochim. Biophys. Acta.* 1605:83–95.
2. Ruban, A. V., D. Rees, …, P. Horton. 1992. Mechanism of Δ-pH-dependent dissipation of absorbed excitation-energy by photosynthetic membranes. 2. The relationship between Lhcii aggregation in vitro and Qe in isolated thylakoids. *Biochim. Biophys. Acta.* 1102:39–44.
3. Ruban, A. V., R. Berera, …, R. van Grondelle. 2007. Identification of a mechanism of photoprotective energy dissipation in higher plants. *Nature.* 450:575–578.
4. Holt, N. E., D. Zigmantas, …, G. R. Fleming. 2005. Carotenoid cation formation and the regulation of photosynthetic light harvesting. *Science.* 307:433–436.
5. Ahn, T. K., T. J. Avenson, …, G. R. Fleming. 2008. Architecture of a charge-transfer state regulating light harvesting in a plant antenna protein. *Science.* 320:794–797.
6. Müller, M. G., P. Lambrev, …, A. R. Holzwarth. 2010. Singlet energy dissipation in the photosystem II light-harvesting complex does not involve energy transfer to carotenoids. *ChemPhysChem.* 11:1289–1296.
7. Miloslavina, Y., A. Wehner, …, A. R. Holzwarth. 2008. Far-red fluorescence: a direct spectroscopic marker for LHCII oligomer formation in non-photochemical quenching. *FEBS Lett.* 582:3625–3631.
8. Bode, S., C. C. Quentmeier, …, P. J. Walla. 2009. On the regulation of photosynthesis by excitonic interactions between carotenoids and chlorophylls. *Proc. Natl. Acad. Sci. USA.* 106:12311–12316.
9. Liao, P. N., C. P. Holleboom, …, P. J. Walla. 2010. Correlation of Car S(1) → Chl with Chl → Car S(1) energy transfer supports the excitonic model in quenched light harvesting complex II. *J. Phys. Chem. B.* 114:15650–15655.
10. Ilioaia, C., M. P. Johnson, …, A. V. Ruban. 2008. Induction of efficient energy dissipation in the isolated light-harvesting complex of photosystem II in the absence of protein aggregation. *J. Biol. Chem.* 283:29505–29512.
11. Krüger, T. P. J., V. I. Novoderezhkin, …, R. van Grondelle. 2010. Fluorescence spectral dynamics of single LHCII trimers. *Biophys. J.* 98:3093–3101.
12. Krüger, T. P. J., C. Ilioaia, …, R. van Grondelle. 2011. Fluorescence intermittency from the main plant light-harvesting complex: sensitivity to the local environment. *J. Phys. Chem. B.* 115:5083–5095.
13. Ruban, A. V., A. Young, and P. Horton. 1994. Modulation of chlorophyll fluorescence quenching in isolated light-harvesting complex of photosystem II. *Biochim. Biophys. Acta.* 1186:123–127.

14. Wentworth, M., A. V. Ruban, and P. Horton. 2001. Kinetic analysis of nonphotochemical quenching of chlorophyll fluorescence. 2. Isolated light-harvesting complexes. *Biochemistry.* 40:9902–9908.

15. Kirchhoff, H., H. R. Hinz, and J. Rosgen. 2003. Aggregation and fluorescence quenching of chlorophyll a of the light-harvesting complex II from spinach in vitro. *Biochim. Biophys. Acta.* 1606:105–116.

16. Schaller, S., D. Latowski, …, R. Goss. 2011. Regulation of LHCII aggregation by different thylakoid membrane lipids. *Biochim. Biophys. Acta.* 1807:326–335.

17. Moya, I., M. Silvestri, …, R. Bassi. 2001. Time-resolved fluorescence analysis of the photosystem II antenna proteins in detergent micelles and liposomes. *Biochemistry.* 40:12552–12561.

18. Yang, C. H., S. Boggasch, …, H. Paulsen. 2006. Thermal stability of trimeric light-harvesting chlorophyll a/b complex (LHCIIb) in liposomes of thylakoid lipids. *Biochim. Biophys. Acta.* 1757:1642–1648.

19. Bayburt, T. H., and S. G. Sligar. 2010. Membrane protein assembly into nanodiscs. *FEBS Lett.* 584:1721–1727.

20. Denisov, I. G., Y. V. Grinkova, …, S. G. Sligar. 2004. Directed self-assembly of monodisperse phospholipid bilayer nanodiscs with controlled size. *J. Am. Chem. Soc*. 126:3477–3487.

21. Banerjee, S., T. Huber, and T. P. Sakmar. 2008. Rapid incorporation of functional rhodopsin into nanoscale apolipoprotein bound bilayer (NABB) particles. *J. Mol. Biol.* 377:1067–1081.

22. Bayburt, T. H., Y. V. Grinkova, and S. G. Sligar. 2002. Self-assembly of discoidal phospholipid bilayer nanoparticles with membrane scaffold proteins. *Nano Lett.* 2:853–856.

23. Ritchie, T. K., Y. V. Grinkova, …, S. G. Sligar. 2009. Reconstitution of membrane proteins in phospholipid bilayer nanodiscs. *In* Methods in Enzymology; Liposomes, Pt F. Elsevier Academic Press, San Diego. 211–231.

24. Janssen, J. J. M., P. H. M. Bovee-Geurts, …, W. J. DeGrip. 1995. Histidine tagging both allows convenient single-step purification of bovine rhodopsin and exerts ionic strength-dependent effects on its photochemistry. *J. Biol. Chem.* 270:11222–11229.

25. Peterman, E. J. G., F. M. Dukker, …, H. van Amerongen. 1995. Chlorophyll a and carotenoid triplet states in light-harvesting complex II of higher plants. *Biophys. J.* 69:2670–2678.

26. Degrip, W. J., J. Vanoostrum, and P. H. M. Bovee-Geurts. 1998. Selective detergent-extraction from mixed detergent/lipid/protein micelles, using cyclodextrin inclusion compounds: a novel generic approach for the preparation of proteoliposomes. *Biochem. J.* 330:667–674.

27. van Stokkum, I. H. M., D. S. Larsen, and R. van Grondelle. 2004. Global and target analysis of time-resolved spectra. *Biochim. Biophys. Acta.* 1657:82–104.

28. Boekema, E. J. 1991. Negative staining of integral membrane-proteins. *Micron Microscop. Acta.* 22:361–369.

29. Blanchette, C. D., J. A. Cappuccio, …, T. A. Sulchek. 2009. Atomic force microscopy differentiates discrete size distributions between membrane protein containing and empty nanolipoprotein particles. *Biochim. Biophys. Acta.* 1788:724–731.

30. Ruban, A. V., and P. Horton. 1992. Mechanism of Δ-pH-dependent dissipation of absorbed excitation-energy by photosynthetic membranes. 1. Spectroscopic analysis of isolated light-harvesting complexes. *Biochim. Biophys. Acta.* 1102:30–38.

31. Ruban, A. V., F. Calkoen, …, J. P. Dekker. 1997. Characterisation of LHC II in the aggregated state by linear and circular dichroism spectroscopy. *Biochim. Biophys. Acta.* 1321:61–70.

32. van Oort, B., A. van Hoek, …, H. van Amerongen. 2007. Aggregation of light-harvesting complex II leads to formation of efficient excitation energy traps in monomeric and trimeric complexes. *FEBS Lett.* 581:3528–3532.

33. Johnson, M. P., A. Zia, …, A. V. Ruban. 2010. Effect of xanthophyll composition on the chlorophyll excited state lifetime in plant leaves and isolated LHCII. *Chem. Phys.* 373:23–32.

34. Gilmore, A. M., T. L. . Hazlett, and Govindjee. 1995. Xanthophyll cycle-dependent quenching of photosystem II chlorophyll a fluorescence: formation of a quenching complex with a short fluorescence lifetime. *Proc. Natl. Acad. Sci. USA.* 92:2273–2277.

35. Grinkova, Y. V., I. G. Denisov, and S. G. Sligar. 2010. Engineering extended membrane scaffold proteins for self-assembly of soluble nanoscale lipid bilayers. *Protein Eng. Des. Sel.* 23:843–848.

36. Jennings, R. C., G. Forti, …, F. M. Garlaschi. 1978. Studies on cation-induced thylakoid membrane stacking, fluorescence yield, and photochemical efficiency. *Plant Physiol.* 62:879–884.

37. Chow, W. S., E. H. Kim, P. Horton, and J. M. Anderson. 2005. Granal stacking of thylakoid membranes in higher plant chloroplasts: the physicochemical forces at work and the functional consequences that ensue. *Photochem. Photobiol. Sci.* 4:1081–1090.

38. Naqvi, K. R., T. B. Melo, …, G. Garab. 1997. Comparison of the absorption spectra of trimers and aggregates of chlorophyll a/b light-harvesting complex LHC II. *Spectrochim. Acta A: Molec Biomolec Spectrosc.* 53:1925–1936.

39. Naqvi, K. R., T. B. Melo, and B. B. Raju. 1997. Assaying the chromophore composition of photosynthetic systems by spectral reconstruction: application to the light-harvesting complex (LHC II) and the total pigment content of higher plants. *Spectrochim. Acta A: Molec Biomolec Spectrosc.* 53:2229–2234.

40. Ruban, A. V., A. A. Pascal, and B. Robert. 2000. Xanthophylls of the major photosynthetic light-harvesting complex of plants: identification, conformation and dynamics. *FEBS Lett.* 477:181–185.

41. Das, S. K., and H. A. Frank. 2002. Pigment compositions, spectral properties, and energy transfer efficiencies between the xanthophylls and chlorophylls in the major and minor pigment-protein complexes of photosystem II. *Biochemistry.* 41:13087–13095.

42. Johnson, M. P., and A. V. Ruban. 2009. Photoprotective energy dissipation in higher plants involves alteration of the excited state energy of the emitting chlorophyll(s) in the light harvesting antenna II (LHCII). *J. Biol. Chem.* 284:23592–23601.

43. Robert, B., P. Horton, …, A. V. Ruban. 2004. Insights into the molecular dynamics of plant light-harvesting proteins in vivo. *Trends Plant Sci.* 9:385–390.